Shahwar, Dura; Yoon, Hoon Hahn; Akkanen, Suvi-Tuuli; Li, Diao; Muntaha, Sidra tul; Cherchi, Matteo; Aalto, Timo; Sun, Zhipei

# Polarization management in silicon photonics

*Published in:*
npj Nanophotonics

*DOI:*
10.1038/s44310-024-00033-6

Published: 01/01/2024

*Document Version*
Publisher's PDF, also known as Version of record



*Please cite the original version:*
Shahwar, D., Yoon, H. H., Akkanen, S.-T., Li, D., Muntaha, S. T., Cherchi, M., Aalto, T., & Sun, Z. (2024). Polarization management in silicon photonics. *npj Nanophotonics*, *1*, Article 35. https://doi.org/10.1038/s44310-024-00033-6

npj | nanophotonics

Review

https://doi.org/10.1038/s44310-024-00033-6

# Polarization management in silicon photonics



**Dura Shahwar[1,2] ✉, Hoon Hahn Yoon[3], Suvi-Tuuli Akkanen[2], Diao Li[2], Sidra tul Muntaha[1], Matteo Cherchi[1], Timo Aalto[1] & Zhipei Sun[2] ✉**

Polarization management plays a key role in various applications, such as optical communications, imaging, and sensing. It not only mitigates detrimental effects (e.g., polarization mode dispersion in optical communication) but also enables advanced functionalities, such as polarization multiplexing and optical isolation. Herein, we review the state-of-the-art approaches for on-chip polarization management. Additionally, we discuss strategies for developing non-reciprocal photonic devices and the challenges associated with monolithic integration in photonics circuits.

Silicon photonics is one of the most promising integration platforms for photonics. It is versatile, economical, and present in many cutting-edge technology areas. The origin of silicon photonics can be traced back to the late 1980s and early 1990s to the works of Soref and Petermann[1,2]. Since then, silicon photonics has been developed into waveguide technologies that realize photonic integrated circuits (PICs) with both passive and active functions. While ”silicon photonics” traditionally referred to waveguides with a silicon core, it now also covers other waveguide materials on silicon wafers (such as silicon nitride and other integrated hybrid materials). The main focus of this paper is on silicon-on-insulator (SOI) waveguides. An early breakthrough in silicon photonics was the finding of a shape-dependent and almost size-independent single-mode (SM) condition for rib waveguides. This allowed us to design and fabricate few-micrometer thick silicon waveguides with low loss and SM operation[3]. However, due to higher integration density and better compatibility with standard silicon microelectronics processing, most silicon photonics research later shifted to submicron-scale waveguides[4]. That offers size-based SM operation, few micrometer bending radii, and fast optical modulation. On the other hand, with rib-strip converters[5] and Euler bends[6], the micron-scale waveguides now offer similar integration density, significantly low losses, and birefringence, although less compatibility with advanced microelectronics processes.

Polarization is crucial in both the above mentioned platforms and PICs in general. Waveguide birefringence is the main cause of polarization dependence properties in silicon photonics, and it can be typically split into geometrical and stress-induced birefringence. The geometrical birefringence is particularly strong in submicron silicon waveguides. More specifically, the asymmetric mode field in these waveguides extends enormously over the core-cladding interfaces where the refractive index changes radically. Therefore, these submicron SOI waveguide circuits typically use only one polarization during operation. The stress of the materials in the core and cladding areas can cause additional birefringence in the waveguides. The resulting waveguide birefringence causes polarization mode dispersion during light propagation, which introduces polarization-dependent optical properties, such as polarization-dependent frequency shifts in the peak positions of optical resonators and polarization-dependent losses (PDL)[4,7–10]. Engineering waveguide dimensions (e.g., non-birefringent waveguides[11]) and stress[12] can control the polarization dependence in the waveguides. In theory, designing a zero-birefringence waveguide for sub-micron silicon-on-insulator (SOI) waveguides is feasible. However, even minor variations in the fabrication process can result in significant birefringence. Conversely, micron-scale waveguides have much more relaxed tolerances, making them less susceptible to these issues.

Polarization sensitivity of components can be a problem for some practical applications which can be tackled by using a polarization diversity scheme[13]. It uses a polarization splitter-rotator (PSR) to separate (or combine) the optical components in the two polarization modes and to have all other polarization-dependent components operating at the same polarization. In general, polarization diversity is mandatory for sub-micron-SOI compared to micron-SOI due to strict fabrication tolerances and more susceptibility towards PDL. For polarization diversity scheme, we need Faraday rotators, and polarization splitters. Faraday rotators would be handy building blocks for polarization management in PICs, which would help cope with the sensitivity of many light sources to back-reflections. However, they have proven to be quite challenging to fabricate in silicon photonics due to the difficulty of breaking Lorentz reciprocity in linear waveguides, especially if low losses and broadband operation are needed[14].

Monolithic integration of all these basic building blocks can help scale down the integrated photonic circuits, advancing Moore’s law in photonics[15]. As long as PICs remain simple, the isolators and circulators can be discrete components placed outside the PIC. However, as the PICs become increasingly complex, monolithic integration of these components

[1]VTT Technical Research Centre of Finland, Tietotie 3, Espoo, 02150, Finland. [2]QTF Centre of Excellence, Department of Electronics and Nanoengineering, Aalto University, Espoo, 02150, Finland. [3]Department of Semiconductor Engineering, School of Electrical Engineering and Computer Science, Gwangju Institute of Science and Technology, Gwangju, 61005, Republic of Korea. ✉e-mail: dura.shahwar@vtt.fi; zhipei.sun@aalto.fi

becomes essential. This approach is the only viable solution for incorporating numerous elements into a single PIC while managing the accumulation of back-reflections within the circuit. Currently, the absence of monolithic isolators and circulators is a significant barrier, hindering the use of PICs in many applications where managing back-reflections is critical.

In this review, our focus primarily on polarization management in submicron-scale and micron-scale SOI platforms. We will discuss the origins of birefringence in different waveguide designs and provide a comprehensive analysis of various polarization-related devices (such as polarization splitters (PSs), Faraday rotators, polarization rotators (PRs), isolators, and circulators). Following this discussion, we will also share our perspective on on-chip polarization management and also investigate new applications. The overview of polarization management components in silicon photonics platform is shown in Fig. 1.

## Fundamentals of polarization management in silicon photonics

Understanding the relevant physical phenomena is important for gaining insight into polarization-managing devices. This section introduces waveguide modes[16], birefringence[12], non-reciprocal phenomena[14,17], and Faraday rotation[18,19]. Their physics is briefly discussed to highlight how these phenomena can be used to modify polarization managing devices. Figure 2 shows the basic simulations for geometric birefringence, polarization state representation, and non-reciprocal phenomena.

### Waveguide modes

Here, we concentrate on optical waveguides fabricated on the planar silicon substrates. Such waveguides generally consist of the substrate, bottom cladding, core, and top cladding. They are designed so that the refractive indices of the cladding materials are lower than that of the core, and the bottom cladding is typically thick enough to isolate the core from the substrate optically. This design confines light and thus supports light propagation inside the waveguide. Light propagation is characterized by modes, which typically depend on the wavelength of the light, the dimensions, and the refractive index of the waveguide.[16,20].

Waveguide that can propagate in a waveguide can be broadly classified into two types: transverse electric (TE) and transverse magnetic (TM) modes. The TE modes have their electric field primarily oriented in the x-direction (along the wafer surface and perpendicular to the propagation

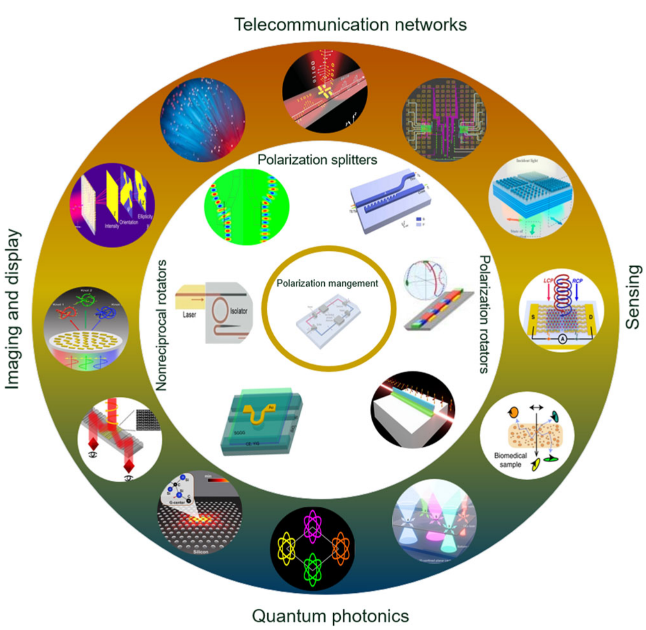


**Fig. 1 | Polarization management components and applications in silicon photonics.** Overview schematic of polarization management components in silicon photonics and their applications[13,86,127,179–192].

direction z). In contrast, TM modes have their electric field mainly in the y-direction (normal to the wafer surface). TE and TM modes typically propagate in the birefringent waveguides with different velocities. If their velocities are different, the phase of the two modes can be determined by using the following simplified equations:

$$\phi_{\mathrm{TE}} = (2\pi/\lambda) n_{\mathrm{TE}} d \tag{1}$$

$$\phi_{\mathrm{TM}} = (2\pi/\lambda) n_{\mathrm{TM}} d \tag{2}$$

where $\lambda$ is the wavelength, $n_{\mathrm{TE}}$ and $n_{\mathrm{TM}}$ are the refractive indices of TE and TM modes, $d$ is the length or the thickness of the material in which light is propagating, and $\phi_{\mathrm{TE}}$ and $\phi_{\mathrm{TM}}$ are the accumulated phase shifts introduced due to the difference in refractive indices and length.

### Birefringence

Birefringence refers to the optical property of some materials that exhibit a difference in refractive index depending on the polarization direction of light passing through them[21]. There are two main sources of modal birefringence for planar optical waveguides: the waveguide geometry (as discussed earlier)[2,11,22] and stress-induced effects[12,23]. The requirement of polarization-insensitive components for telecommunication applications is the primary reason for birefringence control research. Thus, delicate engineering of the waveguide dimensions and stress effects is especially important in polarization management. Note that the intrinsic birefringence of the core and cladding materials is negligible, and the waveguide birefringence only comes from the material boundaries and the stress.

**Geometry-induced birefringence**. Geometry-induced birefringence ($\Delta n_{\mathrm{geo}}$) originates from material geometry. In SOI waveguides, the light is strongly confined, and the waveguide cross-section has the largest influence on the effective index. The common cross-section geometries are slab and ridge waveguides. To accurately control the birefringence and achieve zero birefringence condition[24], some design parameters need to be optimized. For example, the width of ridge waveguides ($W$) is usually chosen to make sure only one mode can propagate. The $\Delta n_{\mathrm{geo}}$ depends on etch depth ($D$) of waveguides, means for the given $W$, $\Delta n_{\mathrm{geo}=0}$ is only achieved with specific value of $D$. Besides $D$, the sidewall angle also affects the $\Delta n_{\mathrm{geo}}$. A small change in sidewall angle or etch depth can have significant impact on waveguide birefringence. The sidewall angle of > 85° is generally required for less demanding fabrication requirements. Another important design parameter is core size of waveguides[25]. The performance of the submicron SOI waveguide platform is more sensitive to fabrication errors due to smaller core size. Nowadays, the best fabrication facilities can control waveguide width and height with ~ 1 nm accuracy, but this is non-ideal for the submicron SOI waveguide platform. Despite high birefringence in submicron silicon waveguides, it is possible to achieve zero birefringence with a specific aspect ratio. Micron-scale waveguides have optical modes mostly confined inside the core that lead to low propagation losses and small polarization dependence compared to the submicron waveguide platform[11]. Figure 2a represents a geometry-induced birefringence calculation for a micron-scale strip waveguide. The results show that strip waveguides have low birefringence at higher widths and that the birefringence becomes almost zero when the waveguide width is ~ 3 µm. Figure 2b represents a geometry-induced birefringence calculation for a submicron strip waveguide. Simulations show that if not designed properly, zero birefringence cannot be achieved.

**Stress-induced birefringence**. Unlike geometry-induced birefringence, stress-induced birefringence ($\Delta n_{\mathrm{stress}}$) in waveguides comes from the stress distribution over the entire waveguide cross-sections. It influences the mode field in the waveguide and is not limited to the material boundaries. Stress-based birefringence in waveguides has been extensively mapped[12,26]. Stress can be caused by various factors such as temperature changes, mechanical strains, or manufacturing defects. It is very

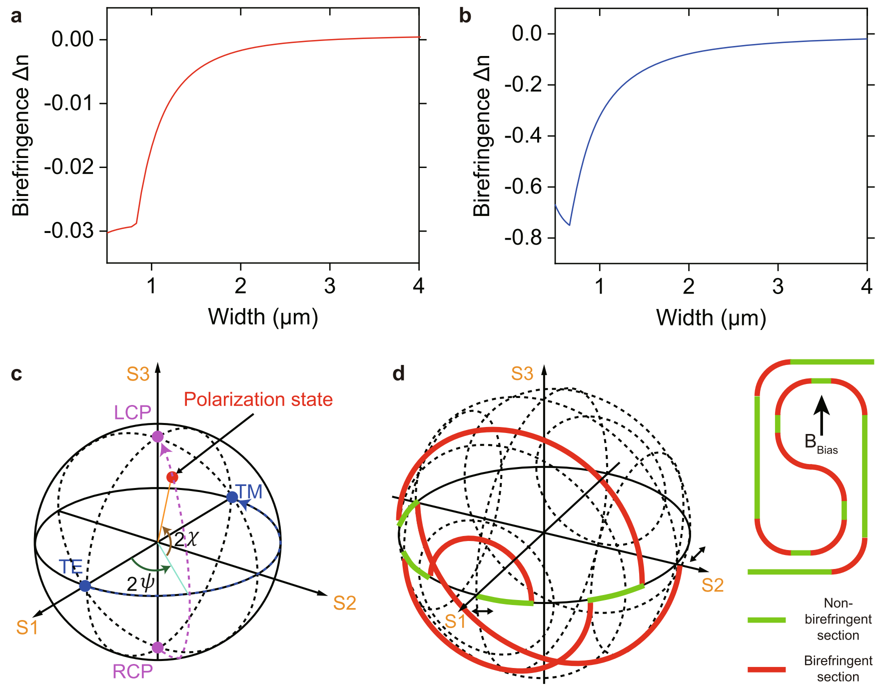


**Fig. 2 | Fundamentals of polarization management.** **a** Geometrical birefringence in a 3 $\mu$m SOI platform. **b** Geometrical birefringence in a sub-micron SOI waveguide (220 nm thickness). **c** Generic representation of polarization states on Poincaré sphere. Linear polarization states are on S1 axis, LCP and RCP are on S3. **d** Poincaré representation of Faraday rotation in silicon waveguides. Red lines present the Euler bends, and green lines present the non-birefringent sections in SOI platform.

hard to avoid stress completely in real fabrication processes, where the wafers are heated and cooled during deposition and etching. Stress-induced birefringence can have positive and negative impacts on waveguide performance. So it is challenging either to remove unwanted- stress or induce the stress to tune birefringence in waveguides. Stress can arise in waveguides due to two main factors: intrinsic stress, which occurs due to the physical properties of the waveguide materials (e.g., the lattice mismatch between adjacent layers), and thermal stress, which is generated during the material growth process and typically negligible in SOI waveguides.

Stress can be controlled and adjust in silicon waveguides using thermal expansion[27] and Laser trimming[28–30] can help to adjust the waveguide birefringence. Among the most studied thermal stress mechanisms in waveguides is their oxide cladding-induced stress. More specifically, birefringence is induced by a thermal layer mismatch influenced by the deposition technique and material composition. The current waveguide fabrication methods typically lead to biaxial stress in the cladding layer, resulting in a change in the refractive index of silicon and the birefringence through the photoelastic effect. The refractive index changes for both polarization states of light due to the photoelastic effect are represented in Equations (3) and (4):

$$\Delta n_x = n_x - n_0 = -C_1\sigma_{xx} - C_2(\sigma_{yy} + \sigma_{zz}) \tag{3}$$

$$\Delta n_y = n_y - n_0 = -C_1\sigma_{yy} - C_2(\sigma_{xx} + \sigma_{zz}) \tag{4}$$

where $C_1$ and $C_2$ are the stress-optical constants, $n_0$ is the refractive index without stress,$\sigma_{xx}$, $\sigma_{yy}$, and $\sigma_{zz}$ are the stress along x, y, and z directions, respectively.

Varying the thickness or deposition techniques can adjust the cladding-induced stress. Hence, waveguide birefringence can be controlled by modifying the cladding thickness, which changes the material's stress. For example, the cladding thickness can be precisely control during the fabrication process. Here cladding term is referred to upper cladding stress as thickness of buried oxide does not have significant effect on waveguide effective index. The stress has a direct relation with $D$ and sidewall angle, but is in inverse relation with $W$. Hence depending on $\Delta n_{geo}$ value, $\Delta n_{stress}$ value can be adjusted to achieve zero or any required birefringence value. In laser trimming technique, the refractive index of silicon waveguides can be modified either e-beam or UV illuminations[31]. This can be useful for many applications e.g., adjusting the phase difference in optical ring resonators or Mach-Zehnder multi/demultiplexer.

## Reciprocal and non-reciprocal phenomena

In a very generic way, the principle of reciprocity states that the response of an optical system or component will remain unchanged even if we change the direction of light propagation. In particular, the principle of reciprocity states that the transfer between optical components input and output waves remains the same, regardless of the polarization or coherence of the incoming light. There are many reciprocity theorems based on their applications. In optics, the most used theorems to explain the phenomena are the Helmholtz reciprocity and Lorentz reciprocity theorem[32]. For reciprocal devices, the Lorentz reciprocity holds. Examples of reciprocal components are polarization splitters and rotators. In contrast to reciprocity, non-reciprocal phenomena defy Lorentz's reciprocity theorem[14]. The theorem holds if the permittivity tensor $\epsilon$ in Equation (5) is asymmetric instead of symmetric, as the off-diagonal elements contribute to non-reciprocal phenomena, such as Faraday rotation[33]. In Equation (5), $\epsilon_{xy}$ is the off-diagonal element of the dielectric tensor, whereas diagonal components ($\epsilon_{xx}$, $\epsilon_{yy}$, $\epsilon_{zz}$) are squares of refractive indices ($n_{xx} = n_{yy} = n_{zz} = n$).

$$\epsilon = \begin{pmatrix} \epsilon_{xx} & \iota\epsilon_{xy} & 0 \\ -\iota\epsilon_{xy} & \epsilon_{yy} & 0 \\ 0 & 0 & \epsilon_{zz} \end{pmatrix} \tag{5}$$

In practice, the permittivity can be made asymmetric by, for example, breaking the time-invariance of the medium by introducing nonlinearity into the system[33] and using magneto-optic materials[34,35].

## Faraday rotation

Faraday rotation is an example of a nonreciprocal phenomenon. Linearly polarized light is a superposition of left and right circular polarized light. In the presence of a magnetic field, the difference in velocities of these components rotates the plane of polarization, which leads to Faraday rotation. Circularly polarized modes are eigenmodes for Faraday rotation, just like the

TE and TM modes are eigenmodes for waveguide polarization evolution. To achieve Faraday rotation in waveguides, coupling between two orthogonal modes is essential. Faraday rotation is associated with the $\epsilon_{xy}$ term of the permittivity tensor:

$$\epsilon_{xy} = 2n_o/k_o\theta_f, \theta_f = VBl \tag{6}$$

where $\theta_f$ is related to the verdet constant $V$, $n_o$ is the refractive index and $k_o$ is the vacuum wavenumber. $B$ is the magnetic field and $l$ is the length of the medium where light will transfer. Using silicon waveguides as Faraday rotators for optical isolators has been investigated. The demonstrated all-silicon Faraday rotator exhibited 1 dB isolation only, due to the effect of birefringence in a straight section of the silicon waveguide[18]. A 6 cm long silicon waveguide is required to achieve Faraday rotation. As reported earlier, a folded waveguide design can be used for the compact design. This type of structure consists of a straight waveguide section and 180 degree Euler bends. The Faraday rotation will accumulate in a straight section, and light will stay linearly polarized, whereas U-bends will add 180 degree phase shift. If any phase shift is added due to the birefringence waveguide section, it will degrade the device's performance. Thus, it is important to design the structure to minimize the effect of birefringence.

The polarization of light can be explained in terms of different systems e.g., Jones vector, polarization ellipse, and Stokes vectors. It is easy to explain Faraday rotation with the help of the Poincaré sphere, which is often used to represent the polarization states of light graphically. The Poincaré sphere is then linked with Stokes polarization parameters $S_1$, $S_2$, $S_3$, where $S_1$ represents the linear horizontal/ vertical polarized light, $S_2$ represents the linear ± 45° polarized light, and $S_3$ represents the left and right circular polarized light[21,36,37]. Linearly polarized states lie on the equator, while the left and right circular polarized light lies on the north and south poles of the Poincaré sphere. Elliptically polarized light is represented anywhere else on the sphere. The Poincaré representation of different polarization states rotation is presented in Fig. 2c. The orientation angle ($\psi$) and ellipticity angle ($\chi$) can be used to define the longitude ($2\psi$) and latitude ($2\chi$) coordinates on the surface of a Poincaré sphere. Figure 2d (left panel) shows the Poincere representation of Faraday rotation in silicon waveguides (right panel). The green lines in the figure indicate the straight waveguide section with zero birefringences and Euler bends for phase shifts. If the light stays linearly polarized over the whole propagation distance, eventually, we will get 45° Faraday rotation, as indicated in Fig. 2d.

## On-chip polarization beam splitters

Polarization beam splitters (PBSs) are a key component in a photonic integration system. PBS's primary function is to differentiate between orthogonally polarized components of a propagating optical beam. On-chip PBSs are typically based on mode evolution[38,39] and mode coupling techniques[40–43]. Mode-evolution technique allows the guided mode to evolve along the waveguide length. Mode-evolution-based devices require to suppress mode-coupling conditions which in turn permits relaxed fabrication tolerances and broadband wavelengths but at the expense of large footprints. The mode-coupling technique involves the transfer of energy between the modes. The mode-coupling-based PBSs require phase-matching conditions, inherent fabrication sensitivity, and more wavelength dependency. Their advantage is a small footprint compared to mode-evolution ones. The small footprint of mode-coupling technique provide ease of integration and they can be easily incorporate into existing photonics systems without requiring significant design changes. The most common mode-coupling techniques are multimode interferometer (MMI)[44,45], directional coupler (DC)[46–48], photonic crystal (PC) structure[49,50], and Mach-Zehnder interferometer (MZI)[51]. The PBSs are usually characterized based on their insertion losses, extinction ratios, bandwidth, and footprint. A comparative analysis of these parameters and design configurations is presented in Table 1.

### Multimode-interferometer-based PBSs

MMIs have been considered a promising structure for on-chip PBSs due to its compact size, wide bandwidth, and large fabrication tolerances. Several MMI structural strategies, including symmetric, asymmetric, and cascaded MMIs[44,52,53], have been demonstrated as viable methods for compact PBS. Figure 3a, b shows the schematics of symmetric and cascaded MMI-based PBSs, respectively. Asymmetric MMI devices can be designed by making minor structural adjustments and dramatically changing optical fields. resulting in a dramatic change in optical fields. Introducing asymmetry in the waveguide length or width manipulates the optical modes' behavior. The length of the MMI coupler has to be multiple of the first self-imaging lengths for both polarization states of light, which is generally difficult to achieve. The advantage of asymmetric MMI-based PBS is that we can achieve any arbitrary power-splitting ratio. They are often cascaded to enhance the extinction ratio with a slight increment in insertion losses[44,53].

### Directional-coupler-based PBSs

On-chip DC-based PBSs can be divided into two categories: symmetric and asymmetric types. Like symmetric MMIs, these structures are typically designed long enough to satisfy the phase-matching conditions. The robustness of symmetric DC is limited by its wavelength-dependent behavior for both polarizations, whereas asymmetric DC exhibits better performance and fabrication tolerance. A proof-of-concept device with low insertion losses (less than 1 dB) and high extinction ratio has been developed[46,54–57]. Figure 3c shows a schematic of two parallel bent waveguides on a submicron SOI platform with different core widths to satisfy phase-matching conditions for TM polarization, whereas the phase-matching condition for TE is not configured[46]. Here, $W_1$ and $W_2$ are the widths of wide and narrow waveguides, whereas $W_g$ is the coupling gap between the two bent waveguides having radius $R_1$ and $R_2$, respectively. Figure 3d shows the schematic of DC-based PBS[56]. By choosing the appropriate coupling length of the coupling region, TM is coupled to the cross port. In this way, TE and TM are separated within a very short length.

### Photonic-crystal-based polarization beam splitter

Researchers also demonstrated the PC-based PBS on submicron SOI where internal PC possesses a photonic gap for one polarization only, reflecting one polarization and transmitting the other polarization state of light. Figure 3e shows the schematic of PC-based PBS[58]. In this type of design, one can eliminate standard multiple requirements and allow independent optimization for each polarization individually.

### Mach-Zehnder-interferometer-based polarization beam splitter

The MZI structure is another compact and simple technique[59] for integrated PBSs, which can be designed without submicron gaps and fabricated via general lithography processes[60]. In general, MZI-based PBS consists of a power divider/combiner and phase shift sections. They have been developed on submicron and micron SOI platforms using MMI couplers. The schematic of MZI-based PBS is presented in Fig. 3f. The input signal is coupled into MMI with width $w_o$ and then split into two arms of equal length $L$ but different widths ($w_1$ and $w_2$). Due to the birefringent waveguide section (with narrow waveguide width $w_1$) in one arm, a phase shift is introduced. The 2 x 2 MMI coupler is then used to combine beams via two arms. The interference between fields with different phases causes one polarization mode to show up at one output, whereas the other polarization mode appears at the other output of MZI. The MZI-based PBSs using form birefringence have been reported on micron SOI platforms[61]. Hence, MZI is a good candidate for PBSs with an acceptable length even when the silicon waveguide has a small birefringence[11] as discussed in Section 2. Another PBS based on the micron scale SOI platform has been proposed using Brewster angles[62] with a footprint of 30 × 30 um$^2$ only. Overall, a large extinction ratio, broad operation bandwidth, and fabrication tolerance are key indicators of well-designed PBSs.

Although all the above-mentioned techniques hold great potential applications in the compact integration of the PICs. However, they have

**Table 1 | Comparative parameters of PBSs using different geometric structures**

| Methods | Extinction Ratio (ER (dB)) | Bandwidth (nm) | Insertion losses (dB) | Length (μm) |
|---|---|---|---|---|
| MMI | 15–20[172], 17–25[173] | 35[173], 40[172] | 1 < [173] | 1034[172] |
| Cascaded MMI | 16[53] | 60[53] | 0.1 dB for TM 0.7 dB for TE[53] | 82.1[53] |
| Photonic crystal | 20[174], 30[58] | 77[174],111[58] | < 2[174], < 3[58] | 77[174], 119.5[58] |
| DC | 15[57], 25 (TM) and 36 (TE)[54] | 72[57] | < 3[54,57] | 14[57] |
| MZI | 15[175] | 35[175] | < 1[175] | 1700[175] |

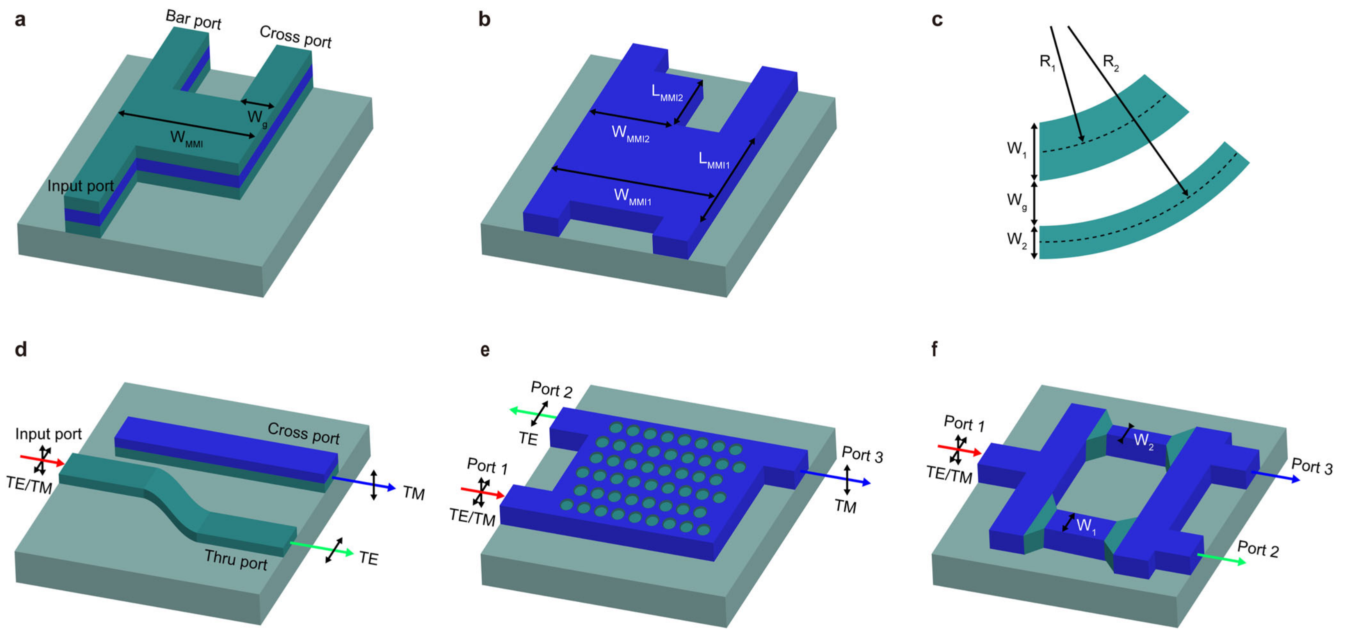


**Fig. 3 | Schematic of on-chip PBSs. a** The schematic of symmetric MMI-based PBS, where $W_g$ is the width of the output port and $W_{MMI}$ is the width of the MMI waveguide[193]. **b** The schematic of a cascaded MMI-based PBS, where $W_{MMI1}$ and $W_{MMI1}$ are the widths of the first and second MMI, respectively, whereas $L_{MMI1}$ and $L_{MMI2}$ are the lengths of the first and second MMI. In this configuration, TM mode is separated at the output port of the first MMI coupler and TE mode at the second coupler. This type of structure enhances the extinction ratio of the device[53]. **c** Two parallel bent waveguides designed to satisfy phase matching conditions. **d** DC-based PBS: where TE and TM are received at bar and cross ports, respectively[56]. **e** PC-based PBS: where TE is reflected back, and TM is transmitted through the output port of MMI[58]. **f** MZI-based polarization splitter in 3 μm SOI platform[61].

their own advantages and dis- advantages. For instance, MMIs are known for their greater fabrication tolerance and simple fabrication process, though they suffer from significant excess loss and imbalance between arms. Compared to MMIs, DCs have short device lengths but they have low tolerance to fabrication errors and need precise gap control between two arms. PCs are compact and efficient but come with complex fabrication, sensitivity to defects, and are limited to specific wavelength ranges. MZIs offer broadband devices with high extinction ratios and are versatile for modulation and switching applications, though they have a large footprint, are sensitive to temperature and require precise phase control. MMI-based PBS are used in broadband wavelength division multiplexers and demultiplexers[63]. DCs and PCs are used in optical sensing, and atomic quantum systems[64]. PCs are in general famous for their nonlinear applications[65].

## On-chip polarization rotators

A PR is a component that rotates the polarization of linearly polarized light to a given angle. Like PBS, on-chip PR normally comes in two different types: mode-evolution[66,67] and mode-coupling[68]. The basic operating principle of mode-evolution and mode-coupling techniques have already been discussed in section 3. PRs, along with PBSs, have been developed on SOI platforms.[69–72]. Like PBS, PRs have also mostly developed on submicron SOI platforms due to the inherent difficulty of introducing sufficient asymmetry and birefringence in micron-scale SOI platforms.

### Mode-evolution-based PRs

Recent demonstrations show that most PRs are based on the mode-evolution technique[73–75]. In mode-evolution-based PR, TE mode is the ground mode of a "horizontal" waveguide core, whereas the TM mode is the ground mode of a "vertical" waveguide core. In this type of PR, the gradual rotation of the core is involved, so breaking the symmetry is required. A slow twist in a waveguide structure will induce polarization rotation, given that the waveguide structure has a large aspect ratio. The upper part of Fig. 4a shows an adiabatic structure design, in which TE or TM is launched, and the lower core is widened gradually[76]. In contrast, the upper layer is designed as a tapered structure. Mode-evolution-based PRs were first described in HIC submicron waveguides[66], in which a pair of waveguide core layers is sufficient to induce polarization rotation. The proposed designs showed no significant wavelength sensitivity over the wavelength span from 1.45 to 1.75 μm. Figure 4b, c shows the schematics of mode-evolution-based PRs with polarization coupling and twisted waveguide, respectively[77,78]. In Fig. 4b, the input waveguide has a width of $W_1$ and is tapered down to $W_2$, which has ground TE mode.

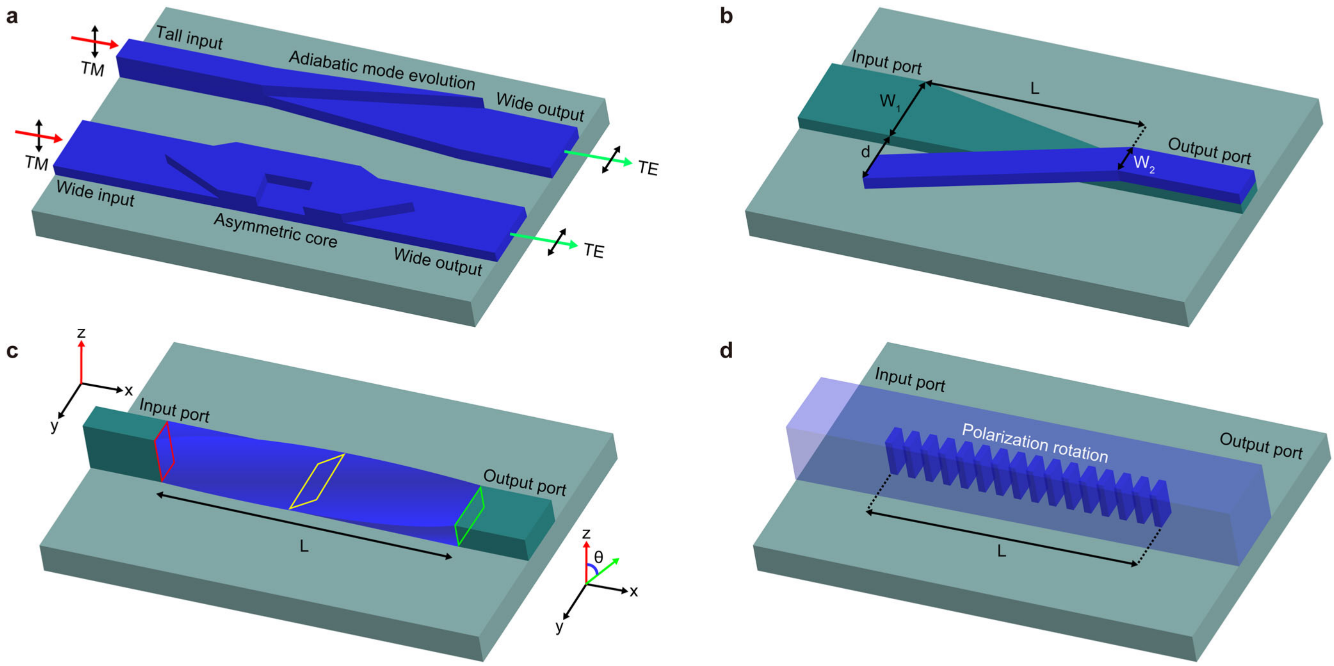


**Fig. 4 | Schematic of on-chip polarization rotators.** **a** Generic schematics for mode-evolution (upper part) and mode coupling-based rotators (bottom part)[76]. **b** Mode-evolution-based polarization coupling[77]. **c** Twisted waveguide based on adiabatic mode conversion[78]. **d** Polarization rotators based on sub-wavelength gratings[67].

**Table 2 | Comparative analysis of different state-of-the-art techniques for polarization rotation**

| Methods | Extinction Ratio (ER (dB)) | Bandwidth (nm) | losses (dB) | Length ($\mu$m) |
|---|---|---|---|---|
| Mode-evolution based PR | 20[176], 22[167], 25[177] | 50[176], 80[167], 100[177] | < 1[176], 1.5[167], 2[177] | 5 × 17[176], 50[177] |
| Mode-coupling based PR | 14.3 (TM) and 29 (TE)[178] | 95[178] | < 1[178] | 5.5[178], 10[71] |

### Mode-coupling based polarization rotators

In mode-coupling-based PR, the TE and TM modes are coupled into the waveguide, in which two orthogonal modes have 50/50 mixed polarization states. Again, for polarization rotation, one needs to break the symmetry for which various approaches have been proposed[79,80]. One method is to partially etch the waveguide, due to the asymmetry and length of the waveguide, TM mode can be converted into TE and vice versa. These components offer high polarization conversion efficiencies and low insertion losses up to 1 dB only but are sensitive to fabrication errors. As mode-coupling-based PRs offer small rotation lengths of up to 10 µm beat length, they are an ideal option for compact devices[71]. The bottom part of Fig. 4a[76], where due to asymmetric core TM is rotated into TE mode, shows the schematic of mode-coupling-based PR. Another example of a PR based on sub-wavelength gratings (SWGs) is shown in Fig. 4d[67]. This geometry is robust to the thickness variation of input and output waveguides and sensitive to a deviation of the SWG duty cycle. This type of mode-coupling-based PR offers, a relatively higher bandwidth than the conventional ones. The comparative analysis of some of the state of art PRs has been presented in Table 2.

However, optimization of polarization management devices is required to achieve better polarization conversion efficiencies, extinction ratios, low losses, and bandwidth. For example, polarization rotators need to have a single guided mode for each polarization to achieve low-loss, high polarization conversion efficiencies. Therefore, during the design optimization process the aspect ratio need to be carefully considered. Moreover, the performance of polarization rotators is often limited by fabrication tolerances specially in mode-coupling based PRs. Using better fabrication methods with 0.05 µm resolution, possibly involving nanotechnology could lead to ultrashort polarization rotators that have conversion efficiency > 96%[67,80]. In mode-evolution techniques, adiabatic conditions need to be optimized for compact and miniature devices[81]. Mode-coupling based PSs are often cascaded to enhance performance e.g., in some design optimizations, DCs are cascaded in two-stage manners which doubles the extinction ratio from 15 dB to 34.3 dB[82]. PS often need high birefringent waveguides specially in thick SOI platform, these waveguides need to be carefully designed as birefringence can significantly vary with waveguide width.

## On-chip non-reciprocal optical components

On-chip non-reciprocal components work on the non-reciprocity phenomena, as discussed in Section 2. Many proposed non-reciprocal components rely on non-reciprocal phase shift (NRPS) and non-reciprocal mode conversion (NRMC) phenomena. NRPS induces phase shift on TM modes using a transverse magnetic field and is the difference between forward and backward propagation constants[83,84] using MZI and ring resonator geometries. Previously, passive non-reciprocal devices based on NRPS were believed to work only for TM polarization[85,86]. Some attempts have been made to operate in TE mode[87], but these devices include full or half reciprocal mode conversion. This means that the first TE mode is converted into TM, enabling NRPS, and then again to TE mode. On the other hand, NRMC is the waveguide equivalent of Faraday rotation. First-ever demonstration of passive TE-mode SOI-integrated isolators with a uniform longitudinal magnetization causing Faraday Rotation achieved isolation up to 11 dB[88]. Both NRPS and NRMC provide ways of achieving waveguide-based integrated optical isolators and circulators to avoid back reflections due to on-chip lasers. The most important goal is to enable the monolithic integration of non-reciprocal components with existing foundry processes. Optical isolators and circulators are divided into two major categories: magneto-optical-based (MO) and magnetic-free nonreciprocal components. In the interferometric NRPS design, a magnetic field is applied transverse to the

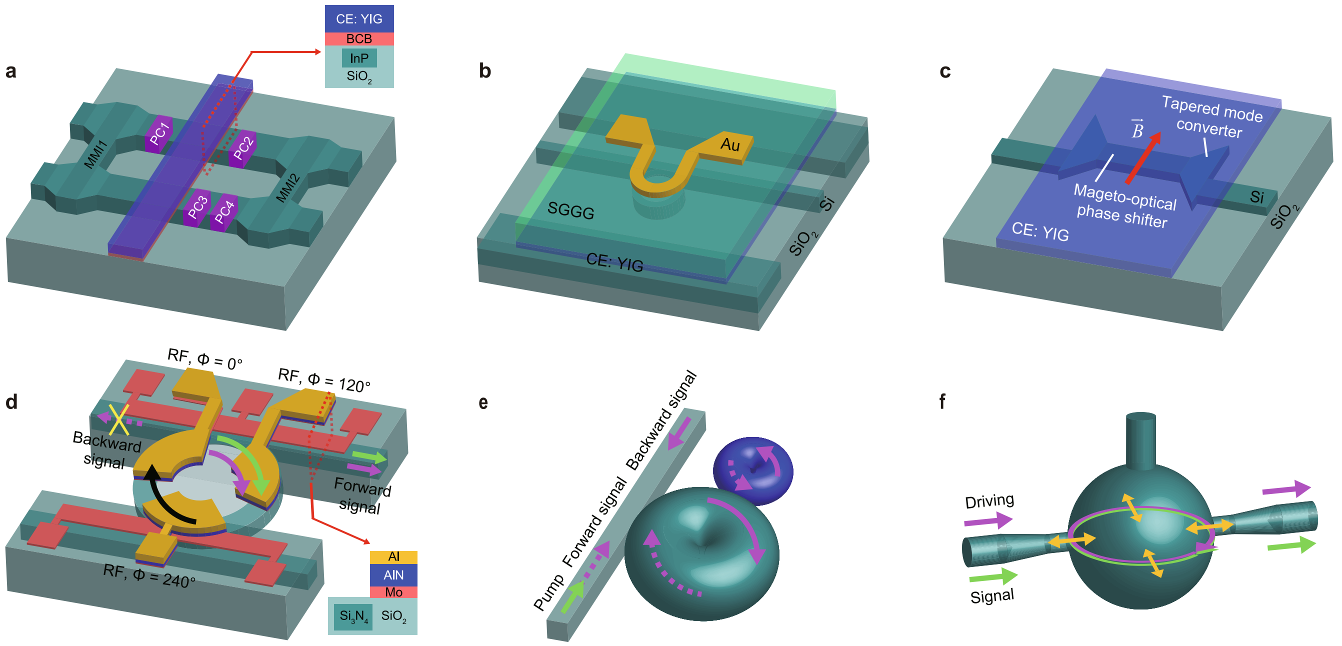


**Fig. 5 | On-chip non-reciprocal components. a** Mach-Zehnder interferometer based polarization-independent isolator/circulator[133]. **b** Integrated Ce: YIG-based isolators on silicon[86]. **c** Structure of the waveguide optical isolator based on direct bonding of Ce: YIG on a silicon waveguide and magnetized using an external magnetic field[134]. **d** A schematic of the acoustic optic isolator. AlN piezoelectric actuators are integrated on top of silicon nitride microring resonators[135]. **e** On-chip optical isolator and nonreciprocal parity-time symmetry empowered by simulated Brillouin scattering with whispering-gallery-mode silica microtoroid resonators[136]. **f** Schematic of optomechanically induced nonreciprocity[117].

waveguide arms, and the phase difference between the two waveguide arms results in constructive interference in the forward direction and destructive interference in the backward direction.

## Optical isolators

Optical isolators allow light propagation in one direction and block it in the opposite direction. The optical isolator has great importance, especially in many systems where one has to avoid back reflections. Figure 5 shows the state of art techniques for on-chip optical isolators.

**Magneto-optical based optical isolators.** Conventionally, optical non-reciprocity is achieved using magneto-optic (MO) materials[89–91]. MO materials are rare-earth garnets of formula $R_3Fe_5O_{12}$, where R is the rare-earth element. These materials are favoured due to their low optical absorption and strong first-order MO effect. These characteristics make MO materials ideal for developing non-reciprocal devices for near-infrared applications (1300 nm to 1550 nm).

The most common MO materials for the development of non-reciprocal components are yttrium iron garnet (YIG), terbium iron garnet (TbIG)[92], Bismuth substituted YIG (Bi: YIG) and cerium-substituted (Ce: YIG). The epitaxial growth of these materials on top of a silicon waveguide is difficult due to lattice mismatch and differences in thermal expansion coefficients. For example, the lattice constant of YIG is 1.238 nm, whereas silicon is 0.543 nm. The thermal expansion coefficient of silicon is $2.33 \times 10^{-6}\ K^{-1}$, whereas YIG is $10.6 \times 10^{-6}\ K^{-1}$ [93]. To evaluate the performance of MO materials, the figure of merit (FoM) must be considered for the Faraday rotation over the loss. For example, FoM of Ce: YIG on Si is 21.8 °$dB^{-1}$ [94], YIG/$Bi_{0.8}$YIG/Si is 397 °$dB^{-1}$, $Bi_{1.5}$YIG/YIG/Si is 769 °$dB^{-1}$[192], $Bi_{0.03}$TbIG is 720 °$dB^{-1}$ [95]. Although YIG crystallizes readily on the non-garnet substrate, it has low Faraday rotation (approximately 100 °$cm^{-1}$ at 1550 nm[94]) compared to TbIG which has Faraday rotation up to 6200 °$cm^{-1}$ [92].

Despite of their strong Faraday rotation effect, the main challenge for waveguide integrated MO devices resides in hybrid integration of MO materials on silicon with existing CMOS compatible technologies. Other than lattice mismatch and thermal mismatch problems, material defects also influence the MO effect and optical losses[15,96]. Two technologies have been developed for hybrid integration of MO materials on silicon 1) deposition techniques[97–101] 2) wafer bonding[102–105]. In deposition method, heterogeneous growth of MO films is done on silicon using chemical vapour phase deposition (CVD)[106], sputtering[107,108] or using pulsed laser deposition[109]. This method has advantage of being scalable, cost effective and compatible with multiple platforms but it has the drawback of process integration issues with many silicon PIC platforms. In wafer bonding method, the MO films are grown on single crystalline garnet or obtained via mechanical lift off techniques[110] and then bonded on silicon waveguides. Compared to the deposition technique, the bonding technique is more advantageous because single-crystalline layers processed in separate processes can be used. We still need tight contact between the materials to have sufficient interaction between the light waves and MO material in bonding techniques. To have tight and uniform contact a direct bonding method was developed and contacted films were annealed[111]. The propagation loss of 64 dB/cm was estimated, this shows that smoothness of bonding material interface is of critical importance in this method. Another technique in wafer bonding is adhesive bonding which requires the precise control of adhesive polymer thickness otherwise it will affect the NRPS in MO materials[112]. In conclusion, despite the progresses, several challenges remain in hybrid integration of MO materials on silicon waveguides[113].

**Magnet-free optical isolators.** Magnetic-free isolators have been demonstrated to break Lorentz reciprocity and time-reversal symmetry to overcome the bottlenecks of magneto-optic materials. So far, it has been achieved through optical nonlinearities[114–116], optomechanically induced transparency[117,118], synthetic magnetic field[119,120], stimulated Brillouin scattering[121–123], and spatio-temporal modulation[124,125]. Each of these types has some advantages and challenges. For example, nonlinearity-based isolators can work without active modulation, but in the case of strong forward signals, the isolator cannot suppress the

**Table 3 | On-chip optical isolators**

| Type | Scheme structure | Mode | Performance (dB) | | Footprint |
|---|---|---|---|---|---|
| | | | Isolation | loss | |
| with magnet | MZI | TE and TM[15] | 30[15] | 5-6 (TM), 9 (TE)[15] | 0.87 × 0.34 $mm^2$(TE), 0.94 × 0.33 $mm^2$(TM)[15] |
| | Ring resonator | TM[86,94] | 19.5[94], 32[86] | 10[86] | 0.15 × 0.07 $mm^2$ [86] |
| | Phase shifter | TE/TM[134] | 20[134] | 3.2[134] | 1.5 × 1.5 $mm^2$ [134] |
| with magnet | Non-linear | N/A[115] | 20[115], 23[127] | 1.3[115], 4.6[127] | N/A[115] |
| | Synthetic magnetic field | N/A[120] | 13[120] | 1[120] | N/A[120] |

transmission of arbitrarily generated noise in the backward direction, and the device becomes reciprocal. Hence, the device performance is limited by dynamic reciprocity[126]. A recent study demonstrated the integrated passive non-linear isolator. The cross-phase modulation contributes to the refractive index change twice that of the self-phase modulation, and the difference between the two leads to intrinsic non-reciprocity[127]. The optomechanical non-reciprocal devices offer unique advantages of all-optical switching, non-reciprocal frequency conversion, and creating a synthetic magnetic field. Still, they have challenges of limited mechanical resonance and integration with PICs (due to the need for air-cladded, isolated microtoroids). The temporal modulation method has the advantage of being reconfigurable but needs electrical, optical, or acoustic pumping. The stimulated Brillouin scattering approach (an effect due to the nonlinearity of a medium) is known to be non-reciprocal. It involves the resonant coupling of optical waves and propagating acoustic waves to achieve non-reciprocal delays. Further, the advantage of these devices is their bandwidth, which is not limited by the optoacoustic interactions and can be made broader (reaching GHz regimes). A comparative analysis of magnet-based and magnet-free isolators using NRPS and NRMC schemes is shown in Table 3.

### Optical circulators

An optical circulator is a device based on the bidirectional transmission of light. Circulators allow the signals to pass in a uni-rotational fashion between their ports and can separate opposite signal flows. In recent years, an integrated platform containing optical circulators based on a silicon platform has been getting attention. Like optical isolators, optical circulators have been achieved by both magnetic and magnet-free techniques. A waveguide optical circulator, composed of a MZI, is investigated[128,129]. Researchers also investigated the optical circulator based on the direct bonding technique. This type of optical circulator utilizes a nonreciprocal phase shift with a silicon waveguide. In this work, the magneto-optic material is bonded on a silicon layer[130]. An on-chip optical circulator based on an engineered waveguide array is reported[131]. A magneto-optic non-reciprocity is introduced to operate the oscillation modes in the forward and backward propagation directions[131]. Also, polarization rotation was used to build waveguide optical circulators[128,132].

Figure 5 shows the schematics of isolators and circulators discussed in this section. Figure 5a shows the schematic of the MZI optical isolator/circulator. It consists of two MMIs on both sides. It forms a four-port circulator and isolator when considering the port pairs on opposite sides. The polarization converters (PCs) are used to rotate eigenmodes. On top of MZI arms, CE: YIG is adhesively bonded. An NRPS will happen for TM mode. For TE input light, after passing through PC1, the mode is converted into TM mode. NRPS is effective on this TM mode in the upper branch (covered with MO material), in the external transverse magnetic field. Then, after passing through PC2, it will again be converted into TE mode. TE mode is not affected by the NRPS effect in the lower branch. In contrast, PC3 and PC4 are to compensate for the imbalance losses due to PC1 and PC2[133].

Figure 5b is another example of an optical isolator based on MO materials. The device is composed of a microring all-pass filter. Ce: YIG is bonded on SOI and critically coupled to a straight bus waveguide. The propagating constants of clockwise (CW) and counterclockwise (CCW) TM modes are differentiated, and the resulting NRPS splits the resonances of CW and CCW TM modes, achieving the isolation for TM mode. (Ca, Mg, Zr)-substituted gadolinium gallium garnet (SGGG) is used on top of silicon as a substrate for the lattice mismatch[86].

Figure 5 c is the schematic of the optical isolator with the two tapered TE-TM mode converters (works as a 3 dB power divider and as a combiner of TE and TM modes, facilitated by higher TE modes) and MO phase shifter. The whole operating principle of this device is based on the interference between TE and TM mode propagating in the MO phase shifter. This provides one-way propagation using NRPS for TM mode. The advantage of this type of geometry is a small footprint compared to MZI, which allows denser integration[134].

Figure 5d represents the schematic example of a magnet-free optical isolator. The reciprocity is broken by the spatio-temporal modulation of ring resonators with acoustic wave resonators. The acoustic wave generates the two co-propagating modes, leading to an indirect interband transition in one direction only[135]. Figure 5e shows a schematic of nonreciprocal parity-time with two toroids coupled together, and the active one is then coupled with fiber. This type of device works on the principle of stimulated Brillion scattering[136]. Figure 5f shows the schematic of optomechanically induced non-reciprocity. It consists of a microring resonator evanescently coupled with tapered fiber. Light interacts with mechanical vibrations and breaks the symmetry between the forward- and back-propagating waves. Such devices typically consist of optical components coupled with mechanical resonators. The mechanical resonators can be membranes or micromirrors, whereas optical components are waveguides or microcavities[117].

## Future perspective

Polarization management is an indispensable technique for the realization of on-chip device performance, not only because the increasing on-chip demand for the handling of birefringence caused polarization-dependent operations (e.g., loss, mode dispersion, wavelength) but also because they can enable new functions for applications. Great efforts and progress have been made in developing on-chip polarization management technologies. These were implemented with several critical functional devices to acquire polarization beam splitting, polarization rotation, optical isolation, and circulation. Various ongoing developments promise to further enhance on-chip polarization management; these will be discussed in the following sub-sections.

### New material platforms

Among the existing SOI platforms, the trade-off with efficiency, footprint, fabrication complexity, and polarization sensitivity is always a significant consideration in a realistic component. Although SOI has gained attention and promises low-cost and high-volume production, indium phosphide (InP) continues to be a popular and advanced PIC platform[137] for polarization management applications[138–140] as shown in Fig. 6a. Silicon nitride (SiN) has also received significant attention as a low-loss passive waveguide PIC platform with optical loss (< 0.01 dB/cm at 700 nm). There are few reports on the SiN platform for polarization applications due to low index contrast between SiN and $SiO_2$ and limited device layer thickness below 1 μm due to film stress[141–143]. Some successful attempts are based on mode evolution techniques, and most of them target $TM_0$-$TE_1$ mode

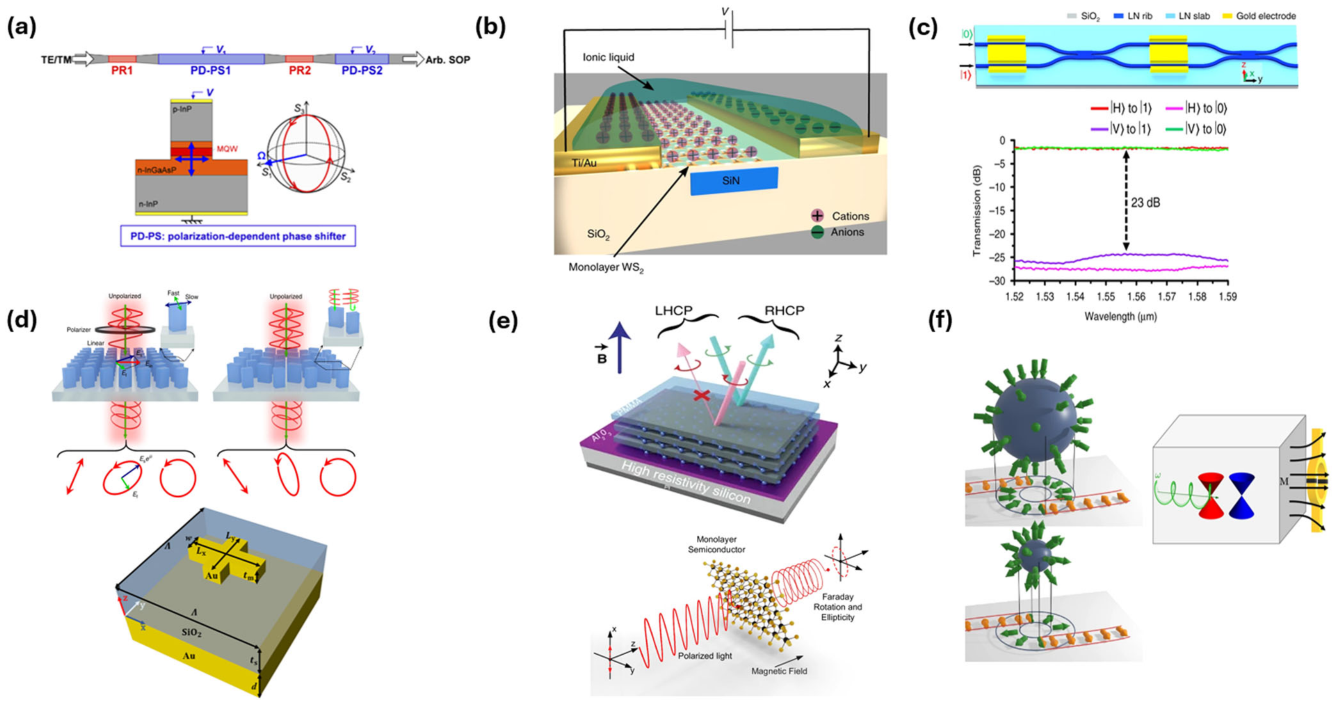

**Fig. 6 | Other conventional material platforms and new avenues for polarization management application.** **a** InP platform for polarization management application. A schematic of polarization control application on InP chip (upper panel) with cross sesction image (bottom panel)[140]. **b** The schematic of polarization splitter and rotator using 2 × 2 Mach-Zehnder interferometer (MZI), composed of two electro-optic (EO) phase shifters (upper panel).The measured transmissions of the device (including the off-chip coupling loss) (bottom panel) on Lithium niobate platform[146]. **c** Illustration of the composite SiN-$WS_2$ waveguide with ionic liquid cladding[145]. **d** Schematic of conventional polarization control based on a cascaded linear polarizer and birefringent single-meta-atom metasurface (left panel). Schematic of the proposed all-in-one polarizer (right panel)[151]. Schematic of the anisotropic metal-insulator-metal meta-atom (bottom panel)[150]. **e** 3D and cross-section of graphene terahertz isolator[158] (upper panel). Schematic of Faraday effect in a 2D monolayer semiconductor[157] (bottom panel) (**f**) Schematic of Weyl fermions[161] (left panel). Weyl semimetals for inverse Faraday rotation[164] (right panel).

conversations instead of $TE_0$-$TM_0$ mode(or vice versa)[144]. A recent work on 2D monolayer materials with SiN platforms can open plethora of application to enable larger scale PICs[145]. A schematic of $WS_2$ and SiN waveguide is shown in Fig. 6b. Lithium niobate (LN) has a strong polarization dependence, which has been used to develop various ridge waveguide-based polarization splitters and rotators[146] as shown in Fig. 6c. However, the state-of-the-art shallow-etch technique is a challenge in the LN platform[147,148]. A recent study demonstrated a large bandwidth (47 nm) on the strip waveguide on an X-cut LN platform[149], showing promise for polarization management applications.

Other than these conventional material platforms, exotic materials (e.g., metamaterials, low-dimensional materials including one-dimensional, two-dimensional (2D) and mixed-dimensional materials, topological materials, etc.) can develop polarization splitters, rotators, and isolators. For instance, metamaterial-based waveplates have been extensively studied[150,151]. An example of conventional metasurface for polarization management application and their integration with silicon is shown in Fig. 6d. Their integration with integrated photonics components can open vast opportunities to achieve broadband and efficient polarization rotation[152,153]. The rectangular lattice of cylindrical silicon Mie resonators was used to efficiently reflect one polarization state and transmit another, hence working as a polarization splitter[154]. This can be used with silicon photonics to miniaturize the polarization splitter designs. 2D materials (e.g., graphene, black phosphorus) have been used to achieve Faraday rotation and waveplates[155–157]. An example of graphene-based terahertz isolator device is presented in Fig. 6e[158]. Incorporating other 2D materials into silicon can significantly reduce footprint size[159]. Further, 2D materials and their heterostructures can be used to miniaturize on-chip spectrometers by diversifying the device's tunability with silicon photonics and minimizing the optical elements[160]. Topological materials (e.g., Weyl semimetals[161], Dirac semimetals) can be used to achieve inverse Faraday rotation due to their non-trivial topology, which has various potential applications (e.g., quantum computing)[162–164] as shown in Fig. 6f. Integrating these exotic materials with conventional CMOS-compatible platforms is still in the early stages of research. Still, they can potentially revolutionize the polarization management field in silicon photonics.

Currently, there is still a need to develop miniature devices and monolithic broadband integration of the aforementioned components when it comes to fully functional PICs in applications where polarization diversity plays a significant role. In addition to the utilization of the SOI platform, the emerging two-dimensional materials with intrinsic in-plane anisotropy and large light-matter interaction along its atomic layer have created a new degree of freedom for the transmission, modulation, detection, and polarization management of light. For instance, tri-layer black phosphorus has been demonstrated as a reconfigurable polarization converter by electrical control, which finds the potential solution for the development of CMOS-compatible polarizers and isolators[165]. Another approach for ultracompact on-chip devices relies on the strong plasmon resonance enhancement in graphene, which enables strong subwavelength confinement and low loss. Combining graphene with resonator resonance provides a new way to realize nonreciprocal high-contrast light isolation[166]. Despite a long way to compete with the well-developed technologies and materials based on traditional SOI platforms, the exciting photonic properties and huge potential in two-dimensional materials have created a new pathway to obtaining on-chip devices with improved indicators, such as performance, footprint, cost, and CMOS compatibility. All these efforts will make the silicon-based PIC more viable for future applications in coherent receivers, polarization multiplexing transmission systems, and sensing.

### New approaches towards polarization management

Current on-chip polarization management methods have advantages and disadvantages. For example, an MMI-based beam splitter is easy to fabricate but has limited bandwidth. A complementary method of using a long MMI is a simple way to improve, but it makes the device miniaturization impossible. Further investigations focus on designing more efficient polarization-independent MMI structures. On the other hand, beam splitters based on directional couplers are usually sensitive to polarization due to the large birefringence in their asymmetric sub-micron waveguides. However, intensive fabrication is crucial to optimize the phase match, as cross-coupling needs to be avoided. In comparison, the MZI structure shows potential in the balance of performances, which has been demonstrated as another optional solution for beam splitters with flexible design, easy fabrication, and compactness. The perspective view of a high-quality beam splitter should consider extinction ratio, broadband operation, and fabrication tolerance, pointing out that the interferometric structure is not an optimal selection when bandwidth is a prior application scenario. An alternative would be a short adiabatic coupler.

Along with the PBSs, PRs, and isolators provide key functionalities for controlling mode polarization and sustaining unidirectional light propagation in the photonics system. Present mode evolution rotators using adiabatic structures generally need a longer size for orthogonal mode coupling, which is not an optimal option for an integrated photonic system. New strategies such as polarization-sensitive plasmonics and mode-interference-based PRs find availability for higher on-chip integration. In addition, techniques such as[167] demonstrates the combination of beam splitting and polarization rotation in one component to obtain arbitrary control of polarization mode, which uses a $TM_0$-$TE_1$ mode converter based on an adiabatic bi-level taper and extends the concept to a polarization splitter-rotator. High polarization extinction ratio, less complicated fabrication, and good compatibility with silicon photonics platforms are the benefits of this method.

Generating a full system function in the integrated photonics circuit also requires unidirectional or bidirectional light propagation, usually realized by optical isolators or circulators. MO materials (such as YIG film) showing a strong Faraday effect or other materials which is capable of suppressing back propagation mode are in the core investigation stage for the current state-of-the-art performance of optical isolators. Although modified epitaxy growth approaches have been demonstrated for Faraday rotation materials, new efforts are made to find low-loss replacements when low energy consumption is vital for practical devices. New proposals should focus on utilizing magnet-free elements in isolators (such as silicon, silicon nitride, and iron garnets). As a counterpart element, an optical circulator becomes more important in silicon-based PIC systems due to the need for bidirectional light transmission. Integration with an MZI interferometer, direct bonding with magneto-optical material, and coupling with a photonic crystal cavity or ring resonator have shown perspectives in silicon waveguide-based on-chip solutions. One of the best solutions is to achieve an all-silicon-based Faraday rotator that does not need any bulk materials.

### Novel applications

On-chip polarization management applications have mainly focused on optical coherent systems, sensors, and quantum photonics. However, its potential extends beyond conventional applications. By exploring diverse applications in silicon photonics, we can harness the benefits of on-chip light manipulation in shaping the future of various technological realms. For instance, one can take advantage of polarization states of light for optical cryptography and polarization-based quantum cryptography. The researchers already demonstrated the chromo-encrypted technique using silver-nanostructured and polarized light[168]. We can combine polarization management applications with bio-photonics, using spectroscopic techniques to detect various diseases and viruses. A recent example of this application is the use of anisotropy of fluorescence light to do the rapid detection of the SARS-CoV-2 RNA[169]. On-chip polarization management components (0˚,45˚, and 90˚ PRs) can make a compact optical detector for military applications[170]. Along with medical, military, and quantum applications, light polarization can be used to enhance data storage density and computing performance. The recent advancements in machine learning and artificial intelligence (AI) demand specialized hardware with more storage and computing speed. For example, researchers demonstrated the techniques to improve data storage density and computing power using nanowires[171]. Based on the above discussion, we can expect numerous applications of on-chip polarization components to be reported in the future.

To conclude, high-performance on-chip silicon photonics PICs have made significant progress in the last decade. Polarization management plays a vital role in achieving these optical systems. The development of state-of-the-art PBSs, PRs, and non-reciprocal components opens a pathway for scaling PICs following Mooreś law in photonics. Advancement in monolithic integration of isolators and circulators will help to maximize the scalability of PICs. However, there are still fundamental challenges to developing magnetless-nonreciprocal components. We expect a bright future due to the existence of novel methods and materials to achieve on-chip polarization splitting, rotation, and Faraday rotation for various applications.

Received: 10 May 2024; Accepted: 15 July 2024;
Published online: 02 September 2024

## References

1. Soref, R. A. & Lorenzo, J. All-silicon active and passive guided-wave components for $\lambda = 1.3$ um and $\lambda = 1.6$ um. *IEEE J. Quantum Electron.* **22**, 873–879 (1986).
2. Soref, R. A., Schmidtchen, J. & Petermann, K. Large single-mode rib waveguides in GeSi-Si and Si-on-$SiO_2$. *IEEE Journal OF Quantum Electronics* **27** (1991).
3. Solehmainen, K. et al. Dry-etched silicon-on-insulator waveguides with low propagation and fiber-coupling losses. *J. Lightwave Technol.* **23**, 3875–3880 (2005).
4. Manolatou, C. & Haus, H. A. Passive components for dense optical integration. *Springer Science and Business Media*. (2002).
5. Aalto, T., Solehmainen, K., Harjanne, M., Kapulainen, M. & Heimala, P. Low-loss converters between optical silicon waveguides of different sizes and types. *IEEE Photonics Technol. Lett.* **18**, 709–711 (2006).
6. Cherchi, M., Ylinen, S., Harjanne, M., Kapulainen, M. & Aalto, T. Dramatic size reduction of waveguide bends on a micron-scale silicon photonic platform. *Opt. Express* **21**, 17814–17823 (2013).
7. Xu, D. et al. Design of polarization-insensitive components using geometrical and stress-induced birefringence in SOI waveguides. *Proceedings of SPIE - The International Society for Optical Engineering* **5730** (2005).
8. Dai, D., Liu, L., Gao, S., Xu, D.-X. & He1, S. Polarization management for silicon photonic integrated circuits. *Laser Phot. Rev.* ***7***, 303–328 (2012).
9. Steinkamp, A., Vorbeck, S. & Voges, E. Polarization mode dispersion and polarization dependent loss in optical fiber systems, optical transmission systems and equipment for WDM networking III. *Proceedings of SPIE - The International Society for Optical Engineering* **5596** (2004).
10. Chen, L., Zhang, Z. & Bao, X. Polarization dependent loss vector measurement in a system with polarization mode dispersion. *Optical Fiber Technol.* **12**, 251–254 (2006).
11. Bera, A., Marin, Y., Harjanne, M., Cherchi, M. & Aalto, T. Ultra-low loss waveguide platform in silicon photonics. In Reed, G. T. & Knights, A. P. (eds.) *Silicon Photonics XVII*, vol. 12006, 1200603. International Society for Optics and Photonics (SPIE, 2022).
12. Winnie, N. Y. et al. Stress-induced birefringence in silicon-on-insulator (SOI) waveguides **5357**, 57–66 (2004).
13. Barwicz, T. et al. Polarization-transparent microphotonic devices in the strong confinement limit. *Nat. Photonics* **1**, 57–60 (2007).

14. Jalas, D. et al. What is — and what is not — an optical isolator. *Nat. Photonics* **7**, 579–582 (2013).
15. Zhang, Y. et al. Monolithic integration of broadband optical isolators for polarization-diverse silicon photonics. *Optica* **6**, 473–478 (2019).
16. Reed, G. T. & Knights, A. P. *Silicon Photonics: an introduction* (Wiley, 2004).
17. Haus, H. A. *Waves and Fields in Optoelectronic* (Prentice-Hall, 1984).
18. Jalas, D. et al. Faraday rotation in silicon waveguides. *IEEE 14th International Conference on Group IV Photonics (GFP)* 141–142 (2017).
19. Sung, S., Qi, X. & Stadler, B. J. H. Garnet waveguides and polarizers for integrated optical isolators on Si substrates. In 2007 4th IEEE International Conference on Group IV Photonics (pp. 1-3). (IEEE, 2007).
20. Saleh, B. E. A. & Teich, M. C. *Fundamentals of Photonics Ch. 6* (Wiley-Interscience, 2007).
21. Hecht, E. *Optics* 5th edn. (Addison-Wesley, 2017).
22. Jalali, B. & Fathpour, S. Silicon photonics. *J. Lightwave Technol.* **24**, 4600–4615 (2006).
23. Huang, M. Stress effects on the performance of optical wavegudies. *Proceedings of SPIE - The International Society for Optical Engineering* (2003).
24. Yusof, N. R. et al. Zero birefringence condition in lithium niobate on insulator rib waveguides. *Adv. Theory Simul.* **7**, 2300853 (2024).
25. Milošević, M. M., Matavulj, P. S., Timotijević, B. D., Reed, G. T. & Mashanovich, G. Z. Design rules for single-mode and polarization-independent silicon-on-insulator rib waveguides using stress engineering. *J. Lightwave Technol.* **26**, 1840–1846 (2008).
26. Born, M. & Wolf, E. *Principles of optics: electromagnetic theory of propagation, interference and diffraction of light* (Elsevier, 2013).
27. Kilian, A., Kirchof, J., Przyrembel, G. & Wischmann, W. Birefringence free planar optical waveguide made by flame hydrolysis deposition (FHD) through tailoring of the overcladding. *J. Lightwave Technol.* **18**, 193–198 (2000).
28. Okuno, M., Sugita, A., Jinguji, K. & Kawachi, M. Birefringence control of silica waveguides on Si and its application to a polarization-beam splitter/switch. *J. Lightwave Technol.* **12**, 625–633 (1994).
29. Will, T., Guan, J., Salter, P. S. & Booth, M. J. Trimming laser-written waveguides through overwriting. *Opt. Express* **28**, 28006–28016 (2020).
30. Sugita, A., Jinguji, K., Takato, N. & Kawachi, M. Laser-trimming adjustment of waveguide birefringence in optical fdm components. *IEEE J. Sel. areas Commun.* **8**, 1128–1131 (1990).
31. De Paoli, G. et al. Laser trimming of the operating wavelength of silicon nitride racetrack resonators. *Photonics Res.* **8**, 677–683 (2020).
32. Potton, R. Reciprocity in optics. *Rep. Prog. Phys.* **67**, 717–754 (2004).
33. Caloz, C. et al. Electromagnetic nonreciprocity. *Phys. Rev. Appl.* **10**, 047001 (2018).
34. Srinivasan, K. et al. High-gyrotropy seedlayer-free Ce:TbIG for monolithic laser-matched soi optical isolators. *ACS Photonics* **6**, 2455–2461 (2019).
35. Karki, D., Stenger, V., Pollick, A. & Levy, M. Broadband bias-magnet-free on-chip optical isolators with integrated thin film polarizers. *J. Lightwave Technol.* **38**, 827–833 (2020).
36. Collett, E. Field guide to polarization. (Bellingham: Spie, 2005).
37. Iizuka, K. *Elements of Photonics, Volume I: In Free Space and Special Media*. Elements of Photonics (Wiley, 2002).
38. Yuan, W. et al. Mode-evolution-based polarization rotator-splitter design via simple fabrication process. *Opt. Express* **20**, 10163–10169 (2012).
39. Watts, M. R., Haus, H. A. & Ippen, E. P. Integrated mode-evolution-based polarization splitter. *Opt. Lett.* **30**, 967–969 (2005).
40. Kojima, K. et al. An mmi-based polarization splitter using patterned metal and tilted joint. *Opt. Express* **20**, B371–B376 (2012).
41. Wang, Z. et al. Experimental demonstration of an ultracompact polarization beam splitter based on a bidirectional grating coupler. Asia Communications and Photonics conference and Exhibition (ACP) (Vol. 2009, pp. 1-7). (IEEE, 2009).
42. Soldano, L. B. et al. Mach-zehnder interferometer polarization splitter in InGaAsP/InP. *IEEE Photonics Technol. Lett.* **6**, 402–405 (1994).
43. Dai, D., Wang, Z. & Bowers, J. E. Ultrashort broadband polarization beam splitter based on an asymmetrical directional coupler. *Opt. Lett.* **36**, 2590–2592 (2011).
44. Jiao, Y., Dai, D., Shi, Y. & He, S. Shortened polarization beam splitters with two cascaded multimode interference sections. *IEEE Photonics Technol. Lett.* **21**, 1538–1540 (2009).
45. Rahman, A., Somasiri, N., Themistos, C. & Grattan, K. Design of optical polarization splitters in a single-section deeply etched mmi waveguide. *Appl. Phys. B* **73**, 613–618 (2001).
46. Dai, D. & Bowers, J. E. Novel ultra-short and ultra-broadband polarization beam splitter based on a bent directional coupler. *Opt. Express* **19**, 18614–18620 (2011).
47. Huang, G., Park, T.-H., Chu, W.-S. & Oh, M.-C. Integrated optic polarization splitter based on total internal reflection from a birefringent polymer. *Opt. Express* **24**, 21012–21019 (2016).
48. Yamazaki, T., Aono, H., Yamauchi, J. & Nakano, H. Coupled waveguide polarization splitter with slightly different core widths. *J. Lightwave Technol.* **26**, 3528–3533 (2008).
49. Tang, Y., Wang, Z., Wosinski, L., Westergren, U. & He, S. Highly efficient nonuniform grating coupler for silicon-on-insulator nanophotonic circuits. *Opt. Lett.* **35**, 1290–1292 (2010).
50. Wang, J., Liang, D., Tang, Y., Dai, D. & Bowers, J. E. Realization of an ultra-short silicon polarization beam splitter with an asymmetrical bent directional coupler. *Opt. Lett.* **38**, 4–6 (2013).
51. Augustin, L., Hanfoug, R., Tol, J., Laat, W. & Smit, M. A compact integrated polarization splitter/converter in ingaasp–inp. *Photonics Technol. Lett., IEEE* **19**, 1286–1288 (2007).
52. Kojima, K. et al. An MMI-based polarization splitter using patterned metal and tilted joint. *Opt. Express* **20**, B371–B376 (2012).
53. Hassan, S., Chack, D. & Mahajan, V. High extinction ratio and low loss polarization beam splitter based on multimode interference for PICS. *Appl. Opt.* **59**, 3369–3375 (2020).
54. Zafar, H. et al. High-extinction ratio polarization splitter based on an asymmetric directional coupler and on-chip polarizers on a silicon photonics platform. *Opt. Express* **28**, 22899–22907 (2020).
55. Dai, S. & Xiao, J. Compact and broadband silicon-based polarization beam splitter using asymmetric directional couplers embedded with subwavelength gratings and slots. *Appl. Opt.* **61**, 126–134 (2022).
56. Wang, D. et al. Broadband and compact polarization beam splitter based on an asymmetrical directional coupler with extra optimizing designs. *Appl. Opt.* **58**, 8221–8226 (2019).
57. Luque-González, J. M. et al. Polarization splitting directional coupler using tilted subwavelength gratings. *Opt. Lett.* **45**, 3398–3401 (2020).
58. Xu, L. et al. Broadband polarization beam splitters based on MMI couplers with internal photonic crystals fabricated using 193nm photolithography. In 2021 Optical Fiber Communications Conference and Exhibition (OFC) (pp. 1-3). (2021).
59. Dai, D., Wang, Z. & Bowers, J. E. Considerations for the design of asymmetrical mach–zehnder interferometers used as polarization beam splitters on a submicrometer silicon-on-insulator platform. *J. Lightwave Technol.* **29**, 1808–1817 (2011).
60. Dai, D., Wang, Z., Peters, J. & Bowers, J. E. Compact polarization beam splitter using an asymmetrical mach–zehnder interferometer based on silicon-on-insulator waveguides. *IEEE Photonics Technol. Lett.* **24**, 673–675 (2012).

61. Shahwar, D., Cherchi, M., Harjanne, M., Kapulainen, M. & Aalto, T. Polarization splitters for micron-scale silicon photonics. InSilicon Photonics XVI Mar 5 (Vol. 11691, p. 1169104). (SPIE, 2021).
62. Elfiqi, A. E., Tanemura, T. & Nakano, Y. Ultracompact polarization beam splitter on multi-micron silicon photonics. *27th OptoElectronics and Communications Conference (OECC) and 2022 International Conference on Photonics in Switching and Computing (PSC)* 1–3 (2022).
63. Mohammed, Z., Paredes, B. & Rasras, M. Cmos compatible ultra-compact mmi based wavelength diplexer with 60 gbit/s system demonstration. *Opt. Express* **30**, 8257–8265 (2022).
64. Hattori, A. et al. Integrated visible-light polarization rotators and splitters for atomic quantum systems. *Opt. Lett.* **49**, 1794–1797 (2024).
65. Zhang, Y., Sheng, Y., Zhu, S., Xiao, M. & Krolikowski, W. Nonlinear photonic crystals: from 2d to 3d. *Optica* **8**, 372–381 (2021).
66. Watts, M. & Haus, H. Integrated mode-evolution-based polarization rotators. *Opt. Lett.* **30**, 138–40 (2005).
67. Chen, J. & Gao, D. Ultra-compact polarization rotator based on mode coupling in a groove-like waveguide, assisted by subwavelength grating. *Appl. Opt.* **59**, 5368–5376 (2020).
68. Liu, B., Shum, P., Zhang, J. & Lo, G. Fabrication tolerance study on mode-coupling-based polarization rotators. In 2010 IEEE International Conference on Communication Systems, pp. 681-684 (IEEE, 2010).
69. Correia, D., da Silva, J. & Hernández Figueroa, H. E. Genetic algorithm and finite element design short single-section passive polarization converter. *Photonics Technol. Lett., IEEE* **15**, 915 – 917 (2003).
70. Vermeulen, D. et al. Silicon-on-insulator polarization rotator based on a symmetry breaking silicon overlay. *Photonics Technol. Lett., IEEE* **24**, 482–484 (2012).
71. Wang, Z. & Dai, D. Ultrasmall Si-nanowire-based polarization rotator. *J. Optical Soc. Am. B* **25**, 747–753 (2008).
72. Aamer, M. et al. Cmos compatible silicon-on-insulator polarization rotator based on symmetry breaking of the waveguide cross section. *IEEE Photonics Technol. Lett.* **24**, 2031–2034 (2012).
73. Zhang, J. et al. An ultracompact surface plasmon polariton-effect-based polarization rotator. *IEEE Photonics Technol. Lett.* **23**, 1606–1608 (2011).
74. Kulik, D. Y., Perov, A. O. & Mospan, L. P. Compact polarization rotators based on the diaphragms with several rectangular apertures (2015).
75. Caspers, J. N., Alam, M. Z. & Mojahedi, M. Compact hybrid plasmonic polarization rotator. *Opt. Lett.* **37**, 4615–4617 (2012).
76. Wim Bogaerts, D. V.*Off-Chip Coupling*, chap. chapter 3 (CRC Press, 2013).
77. Kim, S. & Qi, M. Mode-evolution-based polarization rotation and coupling between silicon and hybrid plasmonic waveguides. *Sci. Rep.* **5**, 18378 (2015).
78. Hou, Z.-S. et al. On-chip polarization rotators. *Adv. Optical Mater.* **7**, 1900129 (2019).
79. Tzolov, V. P. & Fontaine, M. A passive polarization converter free of longitudinally-periodic structure. *Opt. Commun.* **127**, 7–13 (1996).
80. Deng, H., Yevick, D. O., Brooks, C. & Jessop, P. E. Design rules for slanted-angle polarization rotators. *J. Lightwave Technol.* **23**, 432 (2005).
81. Liu, A. et al. The polarization rotator based on adiabatic waveguide. *13th International Conference on Wireless Communications and Signal Processing (WCSP)* 1–4 (2021).
82. Patsamanis, G., Ketzaki, D., Chatzitheocharis, D. & Vyrsokinos, K. Design and optimization of a compact ultra-broadband polarization beam splitter for the scl-band based on a thick silicon nitride platform. *Photonics* **9**, 552 (2022).
83. Hutchings, D. C. et al. Quasi-phase-matched faraday rotation in semiconductor waveguides with a magnetooptic cladding for monolithically integrated optical isolators. *IEEE Photonics J.* **5**, 6602512–6602512 (2013).
84. Bahlmann, N. et al. Improved design of magnetooptic rib waveguides for optical isolators. *J. Lightwave Technol.* **16**, 818–823 (1998).
85. Pintus, P. et al. Microring-based optical isolator and circulator with integrated electromagnet for silicon photonics. *J. Lightwave Technol.* **35**, 1429–1437 (2017).
86. Huang, D. et al. Electrically driven and thermally tunable integrated optical isolators for silicon photonics. *IEEE J. Sel. Top. Quantum Electron.* **22**, 271–278 (2016).
87. Tien, M.-C., Mizumoto, T., Pintus, P., Kromer, H. & Bowers, J. E. Silicon ring isolators with bonded nonreciprocal magneto-optic garnets. *Opt. Express* **19**, 11740–11745 (2011).
88. Zhang, C., Dulal, P., Stadler, B. J. & Hutchings, D. C. Monolithically-integrated TE-mode 1D silicon-on-insulator isolators using seedlayer-free garnet. *Sci. Rep.* **7**, 1–8 (2017).
89. Srinivasan, K. & Stadler, B. J. H. Magneto-optical materials and designs for integrated TE- and uppercaseTM-mode planar waveguide isolators: a review. *Opt. Mater. Express* **8**, 3307–3318 (2018).
90. Stadler, B. J. H. & Mizumoto, T. Integrated magneto-optical materials and isolators: A review. *IEEE Photonics J.* **6**, 1–15 (2014).
91. Srinivasan, K. & Stadler, B. J. H. Review of integrated magneto-optical isolators with rare-earth iron garnets for polarization diverse and magnet-free isolation in silicon photonics. *Opt. Mater. Express* **12**, 697–716 (2022).
92. Fakhrul, T. et al. High figure of merit magneto-optical Ce- and Bi-substituted Terbium iron garnet films integrated on Si. *Adv. Optical Mater.* **9**, 2100512 (2021).
93. Tepper, T. et al. Magneto-optical properties of iron oxide films. *J. Appl. Phys.* **93**, 6948–6950 (2003).
94. Bi, L. et al. On-chip optical isolation in monolithically integrated non-reciprocal optical resonators. *Nat. Photonics* **5**, 758–762 (2011).
95. Fakhrul, T. et al. Magneto-optical Bi:YIG films with high figure of merit for nonreciprocal photonics. *Adv. Optical Mater.* **7**, 1900056 (2019).
96. Pintus, P. et al. An integrated magneto-optic modulator for cryogenic applications. *Nat. Electron.* **5**, 604–610 (2022).
97. Jin, Z., Zhou, H., Zhang, X., Cao, K. & Chen, R. Interface-mediated YIG/Ce:YIG bilayers structure with enhanced magneto-optical properties via pulsed laser deposition. *ACS Mater. Lett.* **5**, 803–810 (2023).
98. Wan, Y. et al. Low-defect-density $WS_2$ by hydroxide vapor phase deposition. *Nat. Commun.* **13**, 4149 (2022).
99. Huang, D. et al. Dynamically reconfigurable integrated optical circulators. *Optica* **4**, 23–30 (2017).
100. Sun, X. Y. et al. Single-step deposition of cerium-substituted yttrium iron garnet for monolithic on-chip optical isolation. *ACS Photonics* **2**, 856–863 (2015).
101. Syouji, A., Higuchi, H. & Tominaga, H. Magneto-optical property of Ce-substituted YIG films fabricated by metal–organic deposition method. *J. Magn. Magn. Mater.* **563**, 169918 (2022).
102. Yokoi, H., Mizumoto, T. & Shoji, Y. Optical nonreciprocal devices with a silicon guiding layer fabricated by wafer bonding. *Appl. Opt.* **42**, 6605–6612 (2003).
103. Yokoi, H. & Mizumoto, T. Proposed configuration of integrated optical isolator employing wafer-direct bonding technique. *Electron. Lett.* **33**, 1787–1788 (1997).
104. Mizumoto, T., Shoji, Y. & Takei, R. Direct wafer bonding and its application to waveguide optical isolators. *Materials* **5**, 985–1004 (2012).
105. Ma, R. et al. Demonstration of an on-chip TE-mode optical circulator. *IEEE J. Quantum Electron.* **59**, 1–7 (2023).

106. Meng, L. et al. Anomalous thickness dependence of curie temperature in air-stable two-dimensional ferromagnetic 1T-CrTe2 grown by chemical vapor deposition. *Nat. Commun.* **12**, 809 (2021).
107. Kotov, V. et al. Enhanced magneto-optic properties in sputtered bi-containing ferrite garnet thin films fabricated using oxygen plasma treatment and metal oxide protective layers. *Materials* **13**, 5113 (2020).
108. Ding, J., Liu, T., Chang, H. & Wu, M. Sputtering growth of low-damping yttrium-iron-garnet thin films. *IEEE Magn. Lett.* **11**, 1–5 (2020).
109. Suzuki, S. et al. Effect of He buffer gas on pulsed Nd: YAG laser deposition of Eu x Y2–x $O_3$ phosphor thin films. *ACS Appl. Electron. Mater.* **4**, 4419–4426 (2022).
110. Gong, Z. Layer-scale and chip-scale transfer techniques for functional devices and systems: a review. *Nanomaterials* **11**, 842 (2021).
111. Shoji, Y., Miura, K. & Mizumoto, T. Optical nonreciprocal devices based on magneto-optical phase shift in silicon photonics. *J. Opt.* **18**, 013001 (2015).
112. Yang, Y., Liu, T., Bi, L. & Deng, L. Recent advances in development of magnetic garnet thin films for applications in spintronics and photonics. *J. Alloy. Compd.* **860**, 158235 (2021).
113. Yan, W. et al. On-chip nonreciprocal photonic devices based on hybrid integration of magneto-optical garnet thin films on silicon. *IEEE J. Sel. Top. Quantum Electron.* **28**, 1–15 (2021).
114. Cao, Q.-T. et al. Reconfigurable symmetry-broken laser in a symmetric microcavity. *Nat. Commun.* **11**, 1–7 (2020).
115. Yang, K. Y. et al. Inverse-designed non-reciprocal pulse router for chip-based lidar. *Nat. Photonics* **14**, 369–374 (2020).
116. Fan, L. et al. An all-silicon passive optical diode. *Science* **335**, 447–450 (2012).
117. Shen, Z. et al. Experimental realization of optomechanically induced non-reciprocity. *Nat. Photonics* **10**, 657–661 (2016).
118. Ruesink, F., Miri, M.-A., Alu, A. & Verhagen, E. Nonreciprocity and magnetic-free isolation based on optomechanical interactions. *Nat. Commun.* **7**, 1–8 (2016).
119. Tzuang, L. D., Fang, K., Nussenzveig, P., Fan, S. & Lipson, M. Non-reciprocal phase shift induced by an effective magnetic flux for light. *Nat. Photonics* **8**, 701–705 (2014).
120. Dostart, N., Gevorgyan, H., Onural, D. & Popović, M. A. Optical isolation using microring modulators. *Opt. Lett.* **46**, 460–463 (2021).
121. Kang, M. S., Butsch, A. & Russell, P. S. J. Reconfigurable light-driven opto-acoustic isolators in photonic crystal fibre. *Nat. Photonics* **5**, 549–553 (2011).
122. Kim, J., Kuzyk, M. C., Han, K., Wang, H. & Bahl, G. Non-reciprocal brillouin scattering induced transparency. *Nat. Phys.* **11**, 275–280 (2015).
123. Merklein, M. et al. On-chip broadband nonreciprocal light storage. *Nanophotonics* **10**, 75–82 (2021).
124. Kittlaus, E. A. et al. Electrically driven acousto-optics and broadband non-reciprocity in silicon photonics. *Nat. Photonics* **15**, 43–52 (2021).
125. Sounas, D. L. & Alu, A. Non-reciprocal photonics based on time modulation. *Nat. Photonics* **11**, 774–783 (2017).
126. Shi, Y., Yu, Z. & Fan, S. Limitations of nonlinear optical isolators due to dynamic reciprocity. *Nat. Photonics* **9**, 388–392 (2015).
127. White, A. D. et al. Integrated passive nonlinear optical isolators. *Nat. Photonics* **17**, 143–149 (2023).
128. Hanashima, N. et al. Hybrid optical circulator using garnet-quartz composite embedded in planar waveguides. *IEEE Photonics Technol. Lett.* **16**, 2269–2271 (2004).
129. Queck, C. K. & Davis, L. E. Broad-band three-port and four-port stripline ferrite coupled line circulators. *IEEE Trans. Microw. Theory Tech.* **52**, 625–632 (2004).
130. Takei1, R. & Mizumoto, T. Design and simulation of silicon waveguide optical circulator employing nonreciprocal phase shift. *Japanese J. Appl. Phys.* **49**, 052203 (2010).
131. El-Ganainy, R. & Levy, M. On-chip multi 4-port optical circulators. *IEEE Photonics J.* **6**, 1–8 (2014).
132. Sugimoto, N. et al. Waveguide polarization-independent optical circulator. *IEEE Photonics Technol. Lett.* **11**, 355–357 (1999).
133. Ma, R. et al. Integrated polarization-independent optical isolators and circulators on an InP membrane on silicon platform. *Optica* **8**, 1654–1661 (2021).
134. Yamaguchi, R., Shoji, Y. & Mizumoto, T. Low-loss waveguide optical isolator with tapered mode converter and magneto-optical phase shifter for te mode input. *Opt. Express* **26**, 21271–21278 (2018).
135. Tian, H. et al. Magnetic-free silicon nitride integrated optical isolator. *Nat. Photonics* **15**, 828–836 (2021).
136. Ma, J. et al. Chip-based optical isolator and nonreciprocal parity-time symmetry induced by stimulated brillouin scattering. *Laser Photonics Rev.* **14**, 1900278 (2020).
137. Lal, V. et al. Extended c-band tunable multi-channel inp-based coherent transmitter PICs. *J. Lightwave Technol.* **35**, 1320–1327 (2017).
138. Soares, F. M. et al. InP-based foundry PICs for optical interconnects. *Appl. Sci.* **9**, 1588 (2019).
139. Ito, M., Fukui, T., Tanemura, T. & Nakano, Y. Compact symmetric polarization rotator-splitter on inp. *Opt. Express* **30**, 4179–4188 (2022).
140. Ito, M. et al. Efficient ingaasp mqw-based polarization controller without active-passive integration. *Opt. Express* **29**, 10538–10545 (2021).
141. Roeloffzen, C. G. et al. Silicon nitride microwave photonic circuits. *Opt. Express* **21**, 22937–22961 (2013).
142. Smith, J. A., Francis, H., Navickaite, G. & Strain, M. J. Sin foundry platform for high performance visible light integrated photonics. *Optical Mater. Express* **13**, 458–468 (2023).
143. Liu, J. et al. High-yield, wafer-scale fabrication of ultralow-loss, dispersion-engineered silicon nitride photonic circuits. *Nat. Commun.* **12**, 2236 (2021).
144. Sacher, W. D. et al. Polarization rotator-splitters and controllers in a $Si_3N_4$-on-SOI integrated photonics platform. *Opt. Express* **22**, 11167–11174 (2014).
145. Datta, I. et al. Low-loss composite photonic platform based on 2d semiconductor monolayers. *Nat. Photonics* **14**, 256–262 (2020).
146. Lin, Z. et al. High-performance polarization management devices based on thin-film lithium niobate. *Light.: Sci. Appl.* **11**, 93 (2022).
147. Noé, R., Koch, B. & Mirvoda, V. $LiNbO_3$-based endless optical polarization control. *2016 21st European Conference on Networks and Optical Communications (NOC)* (2016).
148. Chen, Z., Yang, J., Wong, W.-H., Pun, E. Y.-B. & Wang, C. Broadband adiabatic polarization rotator-splitter based on a lithium niobate on insulator platform. *Photonics Res.* **9**, 2319–2324 (2021).
149. Deng, C. et al. Broadband polarization splitter-rotator on lithium niobate-on-insulator platform. *IEEE Photonics Technol. Lett.* **35**, 7–10 (2023).
150. Deng, Y., Wu, C., Meng, C., Bozhevolnyi, S. I. & Ding, F. Functional metasurface quarter-wave plates for simultaneous polarization conversion and beam steering. *ACS nano* **15**, 18532–18540 (2021).
151. Wang, S. et al. Arbitrary polarization conversion dichroism metasurfaces for all-in-one full poincaré sphere polarizers. *Light.: Sci. Appl.* **10**, 24 (2021).
152. Chen, L. et al. Broadband wave plates made by plasmonic metamaterials. *Sci. Rep.* **8**, 1051 (2018).
153. Deng, Y., Cai, Z., Ding, Y., Bozhevolnyi, S. I. & Ding, F. Recent progress in metasurface-enabled optical waveplates. *Nanophotonics* **11**, 2219–2244 (2022).

154. Slovick, B. A. et al. Metasurface polarization splitter. *Philos. Trans. R. Soc. A: Math., Phys. Eng. Sci.* **375**, 20160072 (2017).
155. Yang, H. et al. Optical waveplates based on birefringence of anisotropic two-dimensional layered materials. *ACS Photonics* **4**, 3023–3030 (2017).
156. Crassee, I. et al. Giant faraday rotation in single-and multilayer graphene. *Nat. Phys.* **7**, 48–51 (2011).
157. Carey, B. et al. Giant faraday rotation in atomically thin semiconductors. *Nat. Commun.* **15**, 3082 (2024).
158. Tamagnone, M. et al. Near optimal graphene terahertz non-reciprocal isolator. *Nat. Commun.* **7**, 11216 (2016).
159. Pelgrin, V., Yoon, H. H., Cassan, E. & Sun, Z. Hybrid integration of 2D materials for on-chip nonlinear photonics. *Light.: Adv. Manuf.* **4**, 168–190 (2023).
160. Yoon, H. H. et al. Miniaturized spectrometers with a tunable van der waals junction. *Science* **378**, 296–299 (2022).
161. Krieger, J. A. et al. Weyl spin-momentum locking in a chiral topological semimetal. *Nat. Commun.* **15**, 3720 (2024).
162. Yan, B. & Felser, C. Topological materials: Weyl semimetals. *Annu. Rev. Condens. Matter Phys.* **8**, 337–354 (2017).
163. Tokman, I. et al. Inverse faraday effect in graphene and weyl semimetals. *Phys. Rev. B* **101**, 174429 (2020).
164. Guo, C., Asadchy, V. S., Zhao, B. & Fan, S. Light control with weyl semimetals. *eLight* **3**, 2 (2023).
165. Biswas, S., Grajower, M. Y., Watanabe, K., Taniguchi, T. & Atwater, H. A. Broadband electro-optic polarization conversion with atomically thin black phosphorus. *Science* **374**, 448–453 (2021).
166. Niu, X. et al. Plasmon-induced transparency effect for ultracompact on-chip devices. *Nanophotonics* **8**, 1125–1149 (2019).
167. Sacher, W. D., Barwicz, T., Taylor, B. J. F. & Poon, J. K. S. Polarization rotator-splitters in standard active silicon photonics platforms. *Opt. Express* **22**, 3777–3786 (2014).
168. Wang, H.-C. & Martin, O. J. Polarization-controlled chromo-encryption. *Adv. Optical Mater.* **11**, 2202165 (2023).
169. Lee, C. Y. et al. Fluorescence polarization system for rapid covid-19 diagnosis. *Biosens. Bioelectron.* **178**, 113049 (2021).
170. Liu, H. et al. The application of space targets polarization detection and recognition. In MIPPR 2019: Remote Sensing Image Processing, Geographic Information Systems, and OtherApplications (Vol. 11432, pp. 234-241) (SPIE, 2020).
171. Lee, J. S., Farmakidis, N., Wright, C. D. & Bhaskaran, H. Polarization-selective reconfigurability in hybridized-active-dielectric nanowires. *Sci. Adv.* **8**, 24 (2022).
172. Huang, Y. et al. High extinction ratio polarization beam splitter with multimode interference coupler on SOI. *Opt. Commun.* **307**, 46–49 (2013).
173. Sun, X., Aitchison, J. S. & Mojahedi, M. Realization of an ultra-compact polarization beam splitter using asymmetric mmi based on silicon nitride / silicon-on-insulator platform. *Opt. Express* **25**, 8296–8305 (2017).
174. Xu, L. et al. Compact broadband polarization beam splitter based on multimode interference coupler with internal photonic crystal for the SOI platform. *J. Lightwave Technol.* **37**, 1231–1240 (2019).
175. Shahwar, D., Cherchi, M., Harjanne, M. & Aalto, T. Polarization splitter based on form birefringence for micron-scale silicon photonics. *ECIO Conference 2020* (2020).
176. Ruan, X., Li, H. & Chu, T. Inverse-designed ultra-compact polarization splitter rotator in standard silicon photonic platforms with large fabrication tolerance. *J. Lightwave Technol.* **40**, 7142–7149 (2022).
177. Li, P. A. et al. An integrated high-extinction-ratio low-loss polarization rotator for silicon photonics across C+L bands. *Conference on Lasers and Electro-Optics (CLEO)* 1–2 (2017).
178. Chen, J. & Xiao, J. Ultracompact silicon-based polarization splitter and rotator based on asymmetric directional couplers with subwavelength gratings. *J. Optical Soc. Am. B* **39**, 345–354 (2022).
179. Sarmiento-Merenguel, J. et al. Demonstration of integrated polarization control with a 40 db range in extinction ratio. *Optica* **2**, 1019–1023 (2015).
180. Zhang, F. et al. Ultra-broadband and compact polarizing beam splitter in silicon photonics. *OSA Contin.* **3**, 560–567 (2020).
181. Tan, Q., Huang, X., Zhou, W. & Yang, K. A plasmonic based ultracompact polarization beam splitter on silicon-on-insulator waveguides. *Sci. Rep.* **3**, 2206 (2013).
182. Guo, R. et al. High–bit rate ultra-compact light routing with mode-selective on-chip nanoantennas. *Sci. Adv.* **3**, e1700007 (2017).
183. Bu, Y. et al. Configurable circular-polarization-dependent optoelectronic silent state for ultrahigh light ellipticity discrimination. *Light.: Sci. Appl.* **12**, 176 (2023).
184. Song, Q. et al. Broadband decoupling of intensity and polarization with vectorial fourier metasurfaces. *Nat. Commun.* **12**, 3631 (2021).
185. He, C. et al. Polarisation optics for biomedical and clinical applications: a review. *Light.: Sci. Appl.* **10**, 194 (2021).
186. Firby, C. J., Chang, P., Helmy, A. S. & Elezzabi, A. Y. Magnetoplasmonic faraday rotators: Enabling gigahertz active polarization control for integrated plasmonics. *ACS Photonics* **3**, 2344–2352 (2016).
187. Intaravanne, Y. et al. Color-selective three-dimensional polarization structures. *Light.: Sci. Appl.* **11**, 302 (2022).
188. Liu, Y. et al. Pixelated filter array for on-chip polarized spectral detection. *Nanomaterials* **13**, 2624 (2023).
189. Giles, M. Explainer: What is quantum communication. *MIT Technol. Rev*. https://www.technologyreview.com/2019/02/14/103409/what-is-quantum-communications/. *Accessed* **6**, 2021 (2019).
190. Liu, Z. et al. Compact stereo waveguide display based on a unidirectional polarization-multiplexed metagrating in-coupler. *ACS Photonics* **8**, 1112–1119 (2021).
191. Redjem, W. et al. All-silicon quantum light source by embedding an atomic emissive center in a nanophotonic cavity. *Nat. Commun.* **14**, 3321 (2023).
192. Abrams, N. C. et al. Silicon photonic 2.5 d multi-chip module transceiver for high-performance data centers. *J. Lightwave Technol.* **38**, 3346–3357 (2020).
193. Rahman, B. M. A., Somasiri, N. P., Themistos, C. & Grattan, K. T. V. Design of optical polarization splitters in a single-section deeply etched mmi waveguide. *Appl. Phys. B* **73**, 613–618 (2001).



## Acknowledgements

Academy of Finland Project Novel optical isolators to continue Moore's law in photonics integration (NOIMO) (Decision number 333980) and the Academy of Finland Flagship Programme, Photonics Research and Innovation (PREIN) (Decision number 346545). This work was supported by the Academy of Finland (grant number: 348920), Research Council of Finland (314810, 333982, 336144, 352780, 352930, and 353364), the Research Council of Finland Flagship Programme (320167,PREIN), the EU H2020-MSCA-RISE-872049 (IPN-Bio), and ERC (834742; 101082183).


## Author contributions

D.S. conceived the study and were responsible for overall direction and planning of the manuscript. The manuscript is originally written by D.S. with the help of H.H.Y. and S.T.A. H.H.Y. made the figures presented in manuscript with the help of D.S. S.T.A and H.H.Y. reviewed edited and improved the manuscript. D.L. specially contributed to the future perspective part. Z.S. and T.A. reviewed and edited the manuscript. S.T.M. and M.C. helped in initial drafting of the paper. All the authors have contributed to the preparation of manuscript. All the work was carried out under the supervision of Z.S.

## Competing interests

The authors declare no competing interests.

## Additional information

**Correspondence** and requests for materials should be addressed to Dura Shahwar or Zhipei Sun.

**Reprints and permissions information** is available at http://www.nature.com/reprints

**Publisher's note** Springer Nature remains neutral with regard to jurisdictional claims in published maps and institutional affiliations.